RSC Advances

ROYAL SOCIETY OF CHEMISTRY

PAPER

View Article Online
View Journal | View Issue

Check for updates

Cite this: *RSC Adv.*, 2025, **15**, 29003

Biochar pre-conditioning reduces nanoplastic toxicity to plant growth-promoting bacteria

Franklin Perez,[a] Yuan Horne Cho,[b] Thomas Sidarta Setio,[c] Dian Yu,[d] Charles Q. Jia,[b] Jane Howe[d] and Ruby May Arana Sullan*[ac]

Received 9th April 2025
Accepted 4th August 2025

DOI: 10.1039/d5ra02482j

rsc.li/rsc-advances

Nanoplastics are emerging environmental pollutants that threaten soil microbial communities, especially plant growth-promoting bacteria. Here, we investigate whether sugar maple biochar—widely recognized for its soil amendment benefits—can reduce nanoplastic toxicity. Using confocal microscopy, scanning electron microscopy (SEM), and fluorescence spectroscopy, we characterized the interactions between biochar and nanoplastics and observed extensive nanoplastic aggregation on biochar surfaces. Pre-conditioning nanoplastics with biochar (*i.e.*, allowing nanoplastics to interact with biochar before bacterial exposure) lowered their effective concentration in solution and reduced surface coverage on bacterial cells. Growth assays confirmed that biochar pre-conditioning improved both planktonic and biofilm growth of *Pseudomonas defensor*, a plant growth-promoting bacteria, at nanoplastic concentrations up to 100 μg mL^{-1}. Our results highlight biochar's potential to sequester nanoplastics and mitigate their toxicity, offering a sustainable strategy for protecting microbial communities in plastic-contaminated soils.

While various nanoparticles have been studied in agricultural soils, nanoplastics (<100 nm) present new challenges related to their potential sources, interactions with soil components and ecological impacts.[1] Compared to larger plastic particles, nanoplastics exhibit distinctive properties—small size, heightened reactivity of adsorbed molecules, and enhanced mobility—that raise concerns about the potential impact of nanoplastic on agriculture.[2,3] Despite growing awareness of plastic pollution, agricultural soils remain exposed to plastics due to continued use of biosolids, mulch, and polymer-coated fertilizers and pesticides.[1]

Several methods such as sludge sorption, filtration and coagulation have been used to remove nanoplastics from the environment.[4] While these approaches have shown success in aquatic environments, immobilizing and sequestering nanoplastics in soil is more challenging and requires different strategies due to the heterogeneity and complexity of opaque soil samples. To this end, bioremediation offers a sustainable solution by leveraging microbial activity to degrade and mitigate nanoparticle pollution. For example, researchers are exploring ways to manipulate the soil microbiome to improve plastic degradation,[5–7] while biofilms have been shown to immobilize nanoparticles within their extracellular matrix without harming the resident microorganisms.[8] Phytoremediation is another eco-friendly strategy, using plant roots to trap nanoparticles.[9,10] However, these approaches have limitations: not all bacteria can effectively degrade nanoplastics,[11] and using crops for remediation can involve significant economic and ecological costs.[10] These drawbacks prompted the need for alternative strategies, leading to the use of biochar as a potential solution for mitigating nanoplastic contamination in agricultural soils.

Biochar, a carbon-rich residue produced through natural or anthropogenic combustion of organic matter, stands out as a promising and eco-friendly approach for addressing nanoplastic pollution.[12] Biochar offers several advantages, including sustainability and biodegradability, which stem from its carbon-rich composition.[13] Moreover, the large surface area and adsorption capacity enable biochar to attract and bind nanoparticles through various mechanisms such as surface adsorption, electrostatic interactions, hydrophobic forces, and complexation.[12–15] In addition, biochar offers multiple agricultural benefits such as increased water retention, improved nutrient availability, and increased microbial diversity, all of which can help offset the toxic effects of nanoplastics on plant and microbial communities.[13,16–18]

Despite the benefits of biochar, the influence of biochar on nanoplastic toxicity in soil bacteria remains unclear. Nanoplastics, known for their potential toxicity to microorganisms,

[a]Department of Physical and Environmental Sciences, University of Toronto Scarborough, 1065 Military Trail, Toronto, ON, Canada. E-mail: ruby.sullan@utoronto.ca
[b]Department of Chemical Engineering and Applied Chemistry, University of Toronto, 200 College St, Toronto, ON, Canada
[c]Department of Chemistry, University of Toronto, 80 St. George St, Toronto, ON, Canada
[d]Department of Materials Science and Engineering, University of Toronto, 184 College St, Toronto, ON, Canada

may alter soil conditions in ways that undermine the protective effects of biochar. Earlier studies have examined biochar–nanoplastic interactions,[12–15,19] biochar–bacteria interactions,[17,18] and nanoplastic–bacteria interactions,[8,20] yet none has tested whether biochar can both immobilize nanoplastics and simultaneously mitigate their detrimental effects on bacterial growth.

Here we address that gap by monitoring the growth kinetics of the plant growth-promoting rhizobacterium (PGPR) *Pseudomonas defensor* after co-exposure to polystyrene nanoplastics and sugar maple biochar. We selected *P. defensor* because it is widely used in biofertilizer formulations; its responses provide a representative model for assessing the agricultural implications of biochar–nanoplastic–bacteria interactions.

Two experimental approaches were tested: (i) introducing biochar, nanoplastics and bacteria all at once ("simultaneous") *versus* (ii) adding biochar to nanoplastic-contaminated media prior to bacterial exposure ("prior"). The simultaneous approach demonstrates whether biochar can immediately bind nanoplastics and protect bacteria, whereas the prior approach evaluates whether biochar can "pre-condition" the environment beforehand, thereby enhancing bacterial resilience and reducing nanoplastic toxicity over time. Contrasting these approaches clarifies how biochar interacts with nanoplastics and soil microbes, providing insights into strategies for improving microbial survival and growth in plastic-contaminated soils.

Materials and methods

Nanoparticle characterization

Unmodified polystyrene (PS) (100 nm), fluorescent amine (PS–NH_2, 100 nm, with an excitation (ex) wavelength of 481 nm and emission (em) wavelength of 540 nm), fluorescent sulfate (PS–SO_4, 100 nm, ex: 538 nm, em: 584 nm), and fluorescence carboxylate (PS–COO^-, 30 nm, ex: 470 nm, em: 505 nm) nanobeads were purchased from Sigma-Aldrich. Nanoparticles were dialyzed as previously reported and concentration determined using UV-vis.[19] Diameters were determined using Dynamic Light Scattering (DLS, NanoBrook Omni, Brookhaven Instruments), and surface zeta potential were measured (Table S1) using Phase Analysis Light Scattering (PALS, NanoBrook Omni, Brookhaven Instruments). FTIR (Bruker Alpha-T FTIR) was used to identify functional groups on the nanoparticle surface. A stock of 500 μg mL^{-1} was prepared in ultrapure water pH 7.2 and kept at 4 °C until use.

Biochar characterization

Sugar maple (*Acer saccharum*) biochar was pyrolyzed at 1000 °C for 24 h, grinded with mortal and pestle, and then sieved through a 53 μm stainless steel mesh drum. A stock of 3 mg per mL biochar was prepared in ultrapure water pH 7.2 and maintained at room temperature. PALS was used to determine surface charge (Table S1). To determine hydrodynamic size of smaller biochar particles, biochar was centrifuged at 500 rpm for 5 min at room temperature and the supernatant was used for DLS measurement. FTIR (Bruker Alpha-T FTIR) was used to identify functional groups on the biochar surface. For more information on biochar preparation and characterization, see our previous articles.[21,22]

Nanoplastic and biochar interaction

To observe nanoplastic interaction with biochar in hydrated conditions, nanoplastic were incubated with biochar in ultrapure water for 30 min, centrifuged at 2000 rpm (402*g*) for 5 min, supernatant removed, washed gently 3× using ultrapure water, and then 5 μL spotted onto a PEI-coated coverslip and flipped onto a glass slide. PS–NH_2, PS–COO^-, and PS–SO_4 were excited using the following lasers, 491 nm, 491 nm, 561 nm, respectively, and images were acquired using an inverted spinning disk confocal microscope equipped with a Spectral Laser Merge Module (WaveFX, Quorum Technologies).

Scanning electron microscopy (SEM, Hitachi SU7000) was used to visualize biochar morphology with 0, 12.5, 50 and 100 μg per mL nanoplastic. The same procedure as confocal was followed except this time, 5 μL spotted onto a 0.1 μm isopore polycarbonate (PC) membrane filter on an SEM stub tape. We verified that 2000 rpm for 5 min sedimented biochar (the absorbance of biochar without nanoplastic is zero) but did not sediment nanoplastic, by determining the change in fluorescence intensity.

To quantify nanoplastic interaction with biochar, the same interaction procedure was followed as SEM and confocal, but this time, 50 μL supernatant were immediately transferred into new microtubes and then transferred into quartz cuvette with 2950 μL ultrapure water for absorbance reading from 200–800 nm in a UV-vis spectrophotometer (Cary 60, Agilent Technologies). The same procedure was followed for fluorescence intensity experiments, but this time 5 μL were transferred into 145 μL ultrapure water in U-shaped 96-well microplate (Greiner) using excitation of 480 nm and emission of 540 nm. Both UV-vis and fluorescence intensity experiments were repeated at least twice with at least three replicates per condition. To assess the effect of temperature on nanoplastic–biochar interactions, fluorescence intensity experiments were also conducted at 4 °C and 30 °C using 50 μg per mL PS–NH_2 and 200 μg per mL biochar, incubated for 2 h. To evaluate the role of salinity, we compared the hydrodynamic size and surface charge of PS–NH_2 under simulated slightly saline conditions (2 dS m^{-1}) and non-saline conditions (no salt), also over a 2 h period. The influence of biochar concentration was also tested by measuring fluorescence intensity after exposing 50 μg per mL PS–NH_2 to low (100 μg mL^{-1}) and high (1600 μg mL^{-1}) biochar concentrations.

Bacterial growth and biofilm formation

P. defensor was grown for 5 h in Luria Broth Lennox (5 g per L NaCl, 10 g per L tryptone, 5 g per L yeast extract) at 27 °C in a static incubator. Bacterial hydrodynamic diameter and surface charge were measured at OD 0.1 using DLS and PALS, respectively. For "simultaneous exposure", bacterial cells were washed 3× using ultrapure water, transferred into a microtube with <53 μm sugar maple biochar and aliquots were transferred into microtubes with nanoplastics to make final concentrations of 0, 12.5, 25, 50, 100 and 200 μg per mL PS–NH_2 with bacterial OD of 0.1 and 0, 100, or 200 μg per mL biochar. Samples were incubated for 30 min, 20 rpm at room temperature, and 5 μL supernatant were transferred into 195 μL fresh LB media in a pre-sterilized microplate. For "prior exposure", biochar was mixed with nanoplastic for 30 min at 20 rpm at room temperature and then centrifuged at 2000 rpm for 5 min. Top 50 μL were immediately transferred into 50 μL bacteria to make final OD 0.1 followed by 30 min incubation, 20 rpm, room temperature. Samples of 5 μL were then transferred into 195 μL fresh LB media in a pre-sterilized microplate and bacterial growth was measured by OD 600 nm every hour for 20 h under static conditions at 27 °C in a microplate reader (Infinite® 200 Pro, TECAN). Maximum growth, lag phase and growth rate were determined using a modified version of the Gompertz fit model.[23] To determine whether media influences bacterial growth after PS–NH_2 interaction, bacteria were also grown in LB Miller (10 g per L NaCl, 10 g per L tryptone, 5 g per L yeast extract), Tryptic Soy Broth (TSB) media (17 g per L tryptone, 3 g per L soytone, 2.5 g per L dextrose, 5 g per L NaCl, 2.5 g per L K_2HPO_4), and King's B (KB) media (20 g per L meat peptone, 1.5 g per L K_2HPO_4, 1.5 g per L $MgSO_4$). For biofilm growth, 10 μL after the 30 min incubation were spotted onto King's B Agar (KBA) and kept in 27 °C static incubator for 1–7 d. Images were acquired using a Samsung Galaxy S8+ cellphone camera. All experiments were repeated at least 3× with at least three replicates for each condition. Biofilm surface coverage was determined using Fiji by using the wand tool to select biofilms.[24] FTIR (Bruker Alpha-T FTIR) was also performed on bacteria to compare functional groups with biochar.

Nanoplastic, bacteria and biochar interaction

Confocal fluorescence microscopy was used to visualize nanoplastic on bacteria in the absence of biochar, as well as under simultaneous and prior exposure conditions, following the procedures described in "Bacterial growth and biofilm formation." To visualize bacterial membranes, cells were stained using 2 μg per mL Nile Red (Thermo Scientific Fischer; excitation, 552 nm, emission: 636 nm). A 5 μL sample was spotted onto a PEI-coated coverslip and images were acquired using an inverted spinning disk confocal microscope equipped with a Spectral Laser Merge Module (WaveFx, Quorum Technologies). Excitation was set to 491 nm for PS–NH_2 and 561 nm for Nile Red, using a 100× oil immersion objective.

Mean intensity was used as an indicator of the amount of nanoplastic retained on the bacterial surface. Mean intensity was determined using Fiji by calibrating images to bacteria without nanoplastic, selecting thresholded nanoplastic and then transferring the selection as a mask onto the original thresholded nanoplastic image.[25] At least 20 cells were analyzed from three images per condition and one-way ANOVA followed by Tukey test were performed on Igor Pro. SEM (Zeiss Sigma 360 VP) was also used to show nanoplastic surface coverage on the membrane during no biochar, simultaneous and prior exposure conditions. After mixing with nanoplastic, bacteria were spotted onto a 0.1 μm PC membrane atop a carbon coated tape on an SEM stub, fixed with 2.5% glutaraldehyde for 1 h, washed 3× using 1× PBS and coated with 20 nm gold.

Results and discussion

Nanoplastic surface charge and functionality influences interaction with biochar

The use of biochar shows promise as a soil amendment for its benefits to plants, soil and bacterial communities. However, it is unclear how the presence of emerging nanomaterial pollutants, such as nanoplastics, might influence these interactions. Biochar is known to effectively bind nanoplastics,[13,15] yet whether biochar can simultaneously immobilize nanoplastics and mitigate their negative effects on bacterial growth remains to be investigated.

Positively charged nanoplastics are generally more toxic to bacteria due to better binding on the bacterial membrane compared to negatively charged nanoplastics leading to one or more detrimental outcomes including reactive oxygen species (ROS) production, membrane damage or inhibition of cell metabolism.[26] We previously showed that positively charged nanoplastics drastically decrease the ability of a plant growth-promoting bacteria to colonize and form biofilms on root surfaces—an effect even more pronounced than their impact on planktonic growth.[20] Here, we investigated if biochar could mitigate the harmful effects of positively charged nanoplastic on bacterial growth.

We started by characterizing the attachment of PS–NH_2 to sugar maple biochar using confocal microscopy, SEM, UV-vis, and fluorescence spectroscopy. We first measured the size and surface charge of nanoplastic, biochar, and bacteria (Table S1). We next verified that the binding of PS–NH_2 to biochar was not artificially caused by centrifugation (to collect the biochar) as nanoplastic concentration in the supernatant did not change when centrifuged in the absence of biochar (Fig. S1). Positively charged nanoplastic interacted with negatively charged biochar particles (<53 μm), resulting in clustered PS–NH_2–biochar aggregates (Fig. 1A). This interaction was dependent on biochar concentration (Fig. S2A) and PS–NH_2 was mostly observed at the periphery of the biochar (Fig. S2B). In addition to positively charged PS–NH_2, biochar–nanoplastic interactions were also observed with negatively charged nanoplastics bearing sulfate and carboxylate functionality (Fig. S3 and S4), as well as with unmodified PS (Fig. S6).

SEM imaging provided a wider field of view and higher resolution for observing nanoplastic interactions with biochar. The biochar was irregularly shaped with a porous matrix and <2 μm-sized crystalline microstructures—formed during biochar processing[22,27]—distributed across the larger biochar surface (Fig. 1B, see Fig. S2C for more SEM images). After a 30 min exposure to PS–NH_2, individual spherical particles could be seen at 12.5 μg per mL PS–NH_2 (Fig. 1B) as well as clusters formed on the biochar surface (Fig. S2C). PS–NH_2 clusters have previously been observed on the biochar surface and their interaction has been described as electrostatic.[19] At 50 (Fig. 1B) and 100 μg per mL PS–NH_2 (Fig. S2C), the biochar surface was

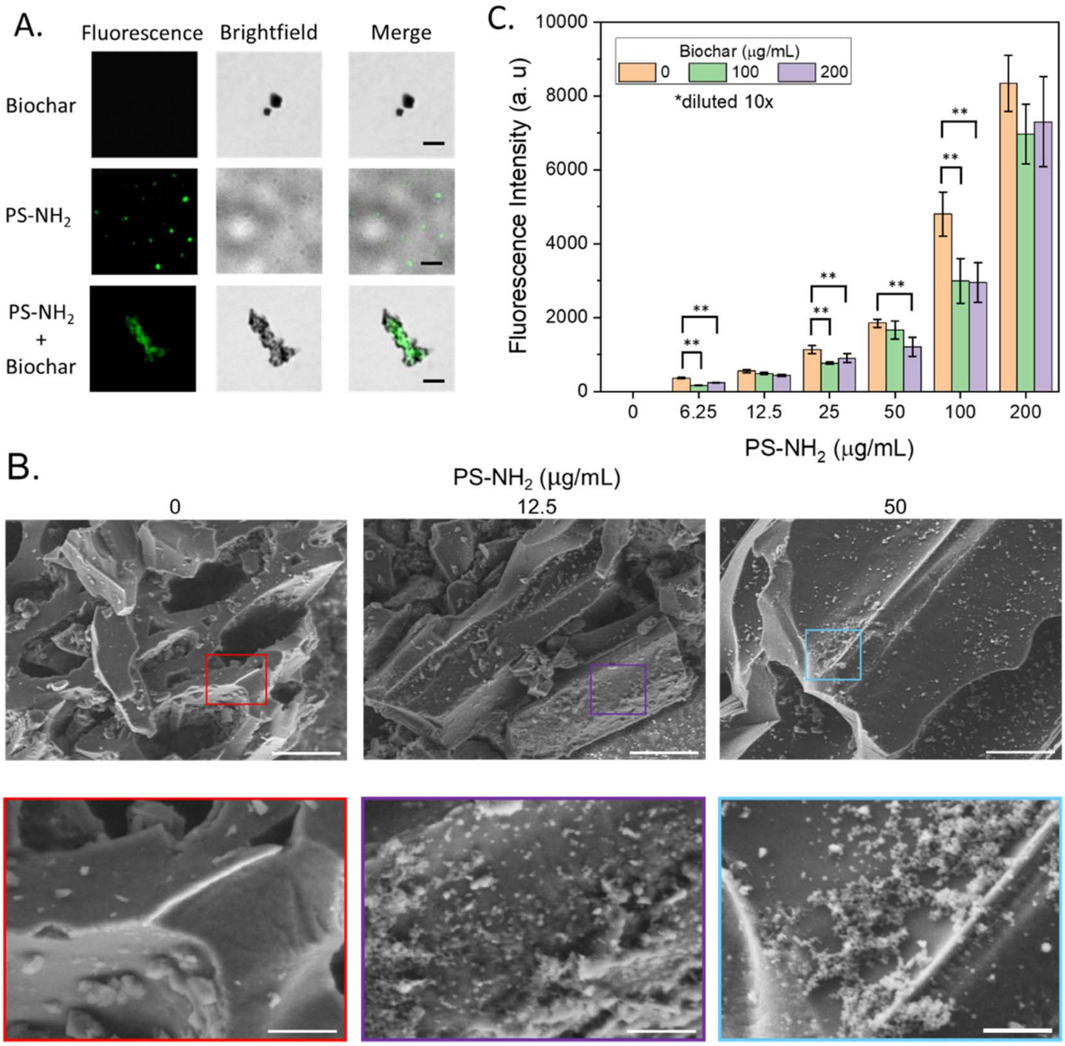

Fig. 1 Interaction of PS–NH_2 with sugar maple biochar. (A) Confocal images of biochar without nanoplastic (top row); 12.5 μg per mL PS–NH_2 without biochar (middle row); 12.5 μg per mL PS–NH_2 with 100 μg per mL biochar (bottom row). (B) SEM images of 0, 12.5 and 50 μg per mL PS–NH_2 with 100 μg per mL biochar. Scale top row: 5 μm, bottom row: 1 μm. (C) Fluorescence intensity of 0–200 μg per mL PS–NH_2 after 0, 100 or 200 μg per mL biochar interaction, diluted 30×. Error bars represent standard deviation of at least six replicates from two trials. One-way ANOVA was used followed by Tukey test where ** represents p < 0.01.

coated with nanoplastic aggregates rather than a homogenous layer across the biochar. Nanoplastics were strongly attached to biochar since they remained adhered despite several washes. In addition, while aggregate formation of positively charged nanoplastic on biochar surface needs further investigation,[28] the interaction of PS–NH_2 with free, <2 μm biochar particles (Fig. 1A) might have promoted aggregation on the surface. This is supported by another study which showed that the formation of nanoplastic primary hetero-aggregates was a requisite before the formation of large structures.[29] This hypothesis is further supported by the presence of 2.3 μm-sized biochar measured with DLS (Table S1) which could have contributed to the decrease in zeta potential (Fig. S5). In contrast to PS–NH_2, SEM showed that PS–SO_4 formed a monolayer at <50 μg mL^{-1} and formed multilayers at 100 μg mL^{-1} on the biochar surface (Fig. S3B). This observation was similar for bare PS nanoplastic, except multilayer formation occurred only at ≥50 μg mL^{-1} (Fig. S6A) and individual spherical particles as well as nanoplastic aggregates were observed at 12.5 μg mL^{-1} similar to PS–NH_2 (Fig. S2B). While 30 nm PS–COO^- were difficult to distinguish from the biochar surface (Fig. S4B), it was also interesting that all types of nanoplastic were on some biochar particles and not on other biochar. This suggests that despite the same processing conditions, individual biochar particles not only display differences in size, but also unique chemical properties making the interaction with nanoplastic variable rather than consistent. To quantify the amount of nanoplastic immobilized by biochar, we first measured the change in absorbance of 12.5–100 μg per mL nanoplastic after interacting with 0, 100, or 200 μg per mL biochar. For control, biochar absorbance after centrifugation was negligible across the measured wavelengths (*i.e.*, zero absorbance). Both 100 and 200 μg per mL biochar reduced the concentration of PS–NH_2 (Fig. S2D–F). These results agreed well using fluorescence intensity with 100 and 200 μg per mL biochar leading to a significant ($p < 0.01$) decrease for majority of PS–NH_2 concentrations (Fig. 1C). Similar to prior reports,[15,19] we also observed negatively charged nanoplastic on biochar. However, biochar only led to a significant decrease in PS and PS–COO^-, but not PS–SO_4 (Fig. S3C, D, S4C, D and S6B) and could be due to differences in biochar types used between the prior reports and our study.

Overall, our results support that nanoplastic interaction with biochar depends on nanoplastic functionality and surface charge, surface properties of biochar, and environmental parameters such as temperature. The conditioning of biochar surfaces by nanomaterials poses interesting biological considerations, including how surface properties influence biochar's role as a microbial carrier, the growth of the associated microbial community and transport of nanomaterials by biochar. As a starting point, the impact of a biochar–nanoplastic system towards bacterial growth remains unclear.[28] While biochar can bind negatively charged nanoplastic, previous experiments showed that positively charged nanoplastic have the most detrimental effect on bacterial growth.[8,20,29] We therefore investigated whether biochar could improve *P. defensor* growth while simultaneously immobilizing PS–NH_2.

Biochar pre-conditioning reduces nanoplastic surface coverage on bacteria

Surface coverage of nanoplastic on the bacterial surface can lead to growth inhibition.[8,20,29] By binding nanoplastic, biochar reduces the amount of nanoplastics available for bacteria, which should lead to an improvement in bacterial growth. First, we simultaneously exposed *P. defensor* to biochar and PS–NH_2 for 30 min. In the first condition, the positive control without biochar or nanoplastics were well dispersed (Fig. 2A, no PS). In the second condition, the negative control with "no biochar" showed PS–NH_2 on bacteria and co-localized with membrane-stained Nile Red. In addition, compared to all other conditions, bacteria in "no biochar" appeared more clustered, which is a well-known response to environmental stress (Fig. S8A for more images). The simultaneous exposure is shown in the third condition, with PS–NH_2 surrounding bacteria similar to "no biochar" although there is less clustering. While nano- and micro-sized biochar particles were bound to bacteria (Fig. S8B), the simultaneous condition was not able to sufficiently reduce nanoplastic binding (Fig. 2B). This suggests that positively charged nanoplastic have a preferential attachment to bacteria rather than biochar despite the bacteria and biochar having a similar negative surface charge (Table S1). For binding of biochar onto bacteria, we hypothesize that initial binding of PS–NH_2 on bacteria could lead to subsequent binding of small biochar particles onto the now positively coated bacterial surface. However, while the specific mechanism as to why PS–NH_2 binds bacteria better than biochar under simultaneous exposure remains to be investigated, *P. defensor* is known to contain various surface appendages including pili and flagella and prior reports suggests bacterial cell surface chemistry such as lipopolysaccharide density and structure in Gram-negative bacteria could play a role in nanomaterial interactions.[30–32]

These results show that biochar does not reduce the nanoplastic binding to bacteria during simultaneous exposure. To test whether biochar can "pre-condition" a nanoplastic-contaminated environment, we first incubated nanoplastics with biochar (Fig. 1) and then introduced bacteria. With this pre-conditioning step, significantly fewer nanoplastics adhered to bacterial cells (Fig. 2). The reduction observed at ≤ 25 μg per mL PS–NH_2 is likely due to nano-sized biochar fragments interacting with the nanoplastics, which lowers their zeta potential and increases their hydrodynamic diameter. This aggregation decreases the effective concentration of free nanoplastics in solution, as shown in Fig. S5 and similarly in Fig. 1A.

Our data suggest the bacterial membrane became saturated at 50 μg mL^{-1} since this was the start of a plateau (Fig. 2B). These results were corroborated with SEM images showing a reduction of nanoplastic on the bacterial surface after biochar pre-conditioning (Fig. 2C). Without nanoplastic, bacteria appeared smooth, and membrane texture could be observed at high magnification (Fig. S9). Without biochar, an evenly distributed monolayer of 12.5 μg per mL PS–NH_2 formed around bacteria which nearly disappeared after biochar pre-conditioning with only a few (Fig. 2C) to hundreds of nanoplastics (Fig. S9) preferentially attached to the peripheral side of the membrane. This observation was consistent at 25 μg per mL PS–NH_2 (Fig. S9) and became less apparent with increasing concentration (Fig. S9). In agreement with confocal microscopy images, simultaneous exposure of bacteria to nanoplastic and biochar did not show a reduction of nanoplastic on the membrane supporting our hypothesis that PS–NH_2 has a greater affinity towards the bacteria than biochar (Fig. S10). In contrast, negatively charged bare polystyrene nanoplastic, or those with either carboxylate or sulfate modifications did not bind bacteria (Fig. S11). It is widely accepted that negatively charged nanoparticles are less efficient in binding negatively charged bacterial surfaces (Table S1) due to electrostatic repulsion.[26,32] To further explore the impact of biochar and nanoplastic exposure on bacteria kinetics, we next performed growth assays.

Biochar pre-conditioning reduces bacterial stress during growth

We have shown that positively charged nanoplastic binds and aggregates from biochar interaction (Fig. 1) resulting in a reduction in bioavailable nanoplastic and a decrease in nanoplastic surface coverage on bacteria (Fig. 2). To determine whether this mechanism could improve bacterial growth, we first established a baseline by exposing cells to 0, 6.25, 12.5, 50, 100 and 200 μg per mL PS–NH_2 without biochar (Fig. 3A, 0 BC). Bacteria exposed to <12.5 μg per mL PS–NH_2 remained unaffected (Fig. 3 and S12). However, bacteria exposed to PS–NH_2 ≥ 12.5 μg mL^{-1} had a significantly lower ($p < 0.05$) maximum growth compared to the control without PS–NH_2 and the growth of bacteria exposed to ≥ 100 μg mL^{-1} was completely inhibited (Fig. 3B). In addition, there was a significant increase in lag phase at PS–NH_2 ≥ 12.5 μg mL^{-1} (Fig. S12B). These results are consistent with previous research on bacteria exposed to

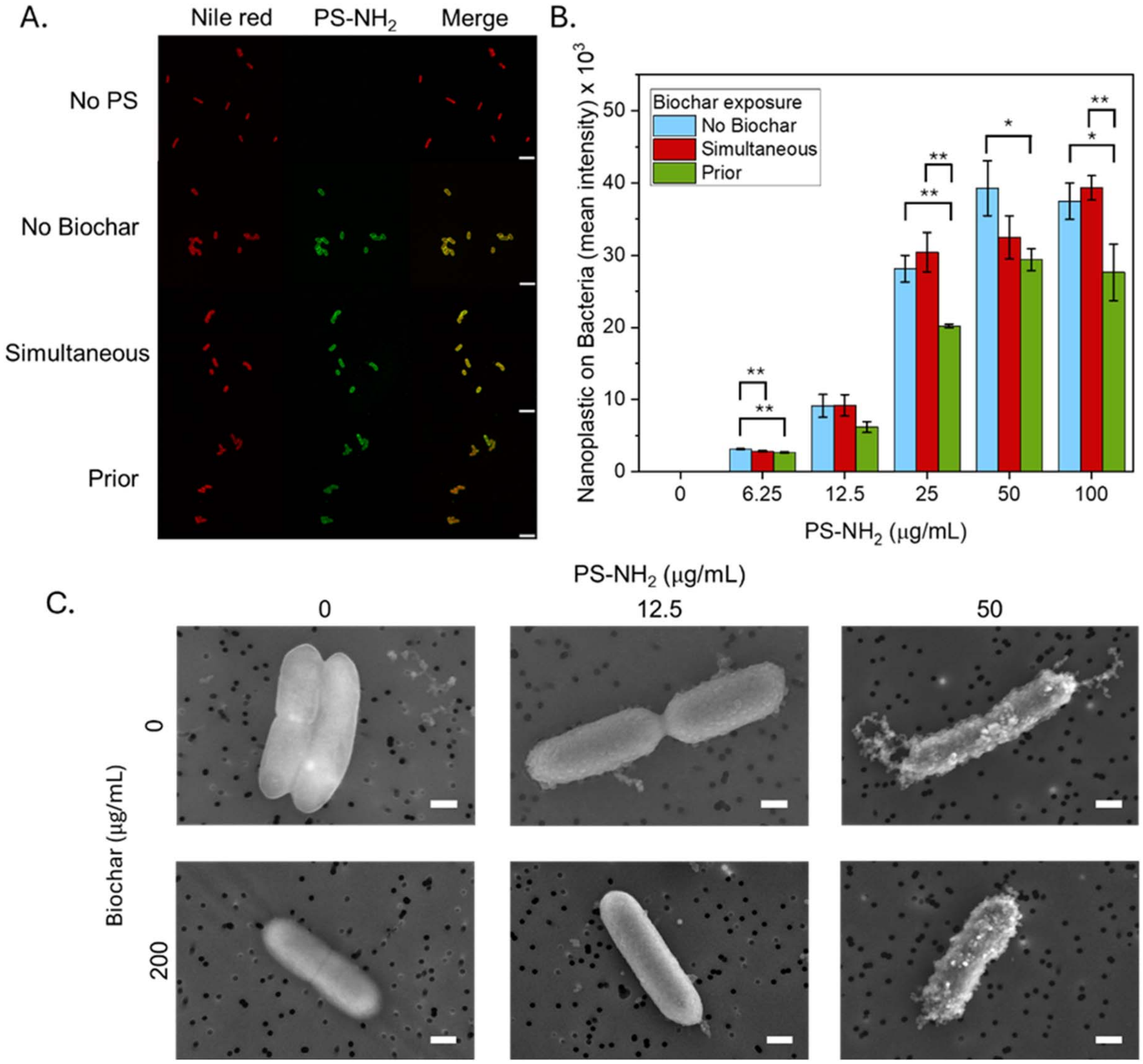

Fig. 2 Biochar reduces nanoplastic on bacterial surface. (A) Confocal microscopy images of bacteria with 0 or 200 μg per mL biochar under simultaneous or prior exposure to 100 μg per mL PS–NH_2. Scale: 5 μm. (B) Nanoplastic fluorescence mean intensity on bacteria with 0 or 200 μg per mL biochar during simultaneous or prior exposure to PS–NH_2. Error bars represent standard deviation of three replicates, where *, **, and *** represent $p < 0.05$, 0.01 and 0.001, respectively, from one-way ANOVA followed by Tukey test. (C) SEM images showing PS–NH_2 on bacteria after prior exposure condition from 0–50 μg per mL PS–NH_2. Scale: 500 nm.

positively charged nanoplastic, where lag phase is increased, and cell death predominantly occurs at higher concentrations in part arising from an increase in nanoplastic surface coverage leading to membrane disruption.[29] Overall, growth rate was least affected by nanoplastic (Fig. S12A), and biochar itself did not impact bacteria (Fig. 3 and S12A, B). This contrasts with another study where bacterial exposure to biochar alone led to an increase in lag phase, longer growth phase and increase in cell density.[17] This was due to a different mechanism, where longer exposure time of bacteria and biochar in media led to adsorption of nutrients in the media onto biochar.[17] While the use of biochar to reduce nanoplastic toxicity was previously reported for plants,[16] the novelty of investigating all three components at once – biochar, nanoplastic, and bacteria, made it difficult to compare conclusions from different studies which investigated only two components.[12,15,17–19] Others have used a different method involving the immobilization of bacteria on biochar to improve removal of environmental contaminants[33–35] and we are currently investigating whether this approach can also improve removal of nanoplastic. Furthermore, while idealized nanoparticles provide information about fundamental interactions, since nanoparticles in the environment are expected to be heterogenous in shape, size, and surface chemistry,[28] future studies should investigate true-to-life nanoplastic interactions with biochar,[36] rather than continue to use monodisperse particles.[14–16] This is important as the interactions of pristine *vs.* aged plastic with biological systems has already been shown to be significant, although these studies[37,38] focussed on aged *microplastic* with soil microbes, whereas aged *nanoplastic* interactions with soil microbes has been

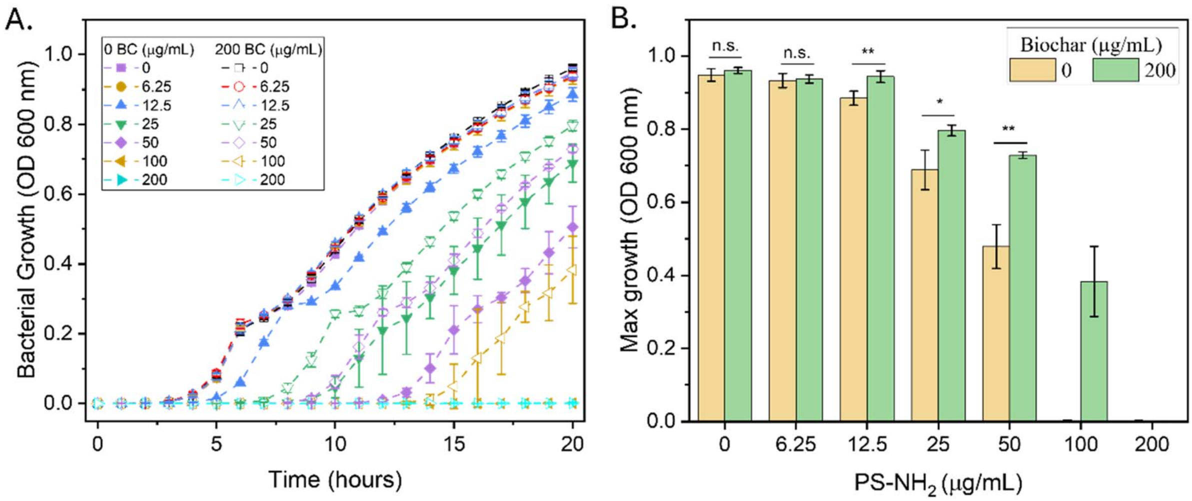

Fig. 3 Biochar pre-conditioning to nanoplastic improves bacterial growth. (A) Bacterial growth for 20 h recorded every hour in nutrient-rich media with 0–200 μg per mL PS–NH_2 with 0 or 200 μg per mL biochar. (B) Maximum growth of bacteria obtained from growth curves in (A). Bars represent standard deviation of at least three replicates from three trials, where n.s. is non-significant, * and ** from *t*-test represent $p < 0.05$ and $p < 0.01$, respectively.

underexplored. A major strength of our study is the lower concentration of biochar used to sequester nanoplastic,[19,36,39,40] which also reduces toxicity towards bacterial growth (Fig. 3).

Once we established the baseline (Fig. 3A), cells were again exposed to PS–NH_2, but this time with prior exposure of up to 200 μg per mL biochar and nanoplastic. Prior interaction of 200 μg per mL biochar with PS–NH_2 reduced the toxicity of nanoplastic to bacteria, indicated by higher max growth (Fig. 3B) and shorter lag phase (Fig. S12B) at ≥12.5 μg mL^{-1}. Additional experiments showed that increasing biochar concentrations restored growth parameters to baseline values (Fig. S12C–E) which correlated well with fluorescence intensity experiments (Fig. S1A). In addition, a comparison of different media revealed that the rate of growth and final density of bacteria was sensitive, whereas the time it took for bacteria to start growing was more tolerant to changes in growth conditions (Fig. S12C–E). This is significant for bacterial biofertilizers since optimizing conditions can improve viability in field trials. Additional FTIR analysis suggested that PS–NH_2 interaction with bacteria mainly through electrostatic and possibly hydrogen bonding was stronger compared to biochar, which likely involved electrostatic and pi–pi interactions (Fig. S7). These results demonstrate biochar's potential to mitigate nanoplastic toxicity to planktonic bacteria. However, many plant bacteria, including *P. defensor*, colonize plant roots as biofilms to fulfill their growth-promoting roles.[41,42] To address this, we next grew biofilms on agar as environmental models after exposure to nanoplastic with or without biochar.

Biochar mitigates nanoplastic toxicity for biofilms at high nanoplastic concentrations

Biofilms play a crucial role in promoting plant health by enhancing nutrient availability, protecting against pathogens, and improving resilience to environmental stressors. To further understand the implications of biochar–nanoplastic interactions in more ecologically relevant contexts, we explored how these interactions influenced biofilm formation after nanoplastic exposure. Fig. 4A shows biofilms on agar after exposure to nanoplastic without or prior exposure to biochar. Without biochar, biofilm formation after 1 d was visibly affected at 50 μg per mL PS–NH_2 and complete inhibition occurred at 100 μg mL^{-1} (Fig. 4A). In contrast, with biochar reducing availability of nanoplastic, biofilms were affected at 100 μg mL^{-1} and inhibition occurred at 200 μg mL^{-1} (Fig. 4A). Since *P. defensor* must cover plant root surfaces to form biofilms which are essential for promoting plant growth, we measured surface coverage on model agar surfaces. Similar to planktonic growth (Fig. 3), biofilms began to be affected at 12.5 μg per mL PS–NH_2 compared to 0 μg per mL PS–NH_2 (Fig. 4B). However, whereas biochar improved planktonic growth parameters starting at 12.5 μg per mL PS–NH_2 (Fig. 3 and S12A, B), biochar mitigated the effect of nanoplastic on biofilm surface coverage only at 50 μg mL^{-1} (Fig. 4B) and allowed colonies to persist at 100 μg per mL PS–NH_2. Despite the early biofilm formation inhibition at high nanoplastic concentrations, biofilms were resilient and formed biofilms similar to those without nanoplastic after 3 d (Fig. 4C). Moreover, the formation of yellow patches on biofilms began at 3 d with 50 μg per mL PS–NH_2 for both "no biochar" and biochar conditions, and biofilms were completely yellow at 100 μg per mL PS–NH_2 for "no biochar" (Fig. 4C). The patches were absent at concentrations ≤25 μg mL^{-1}, which all resembled biofilms without nanoplastic, suggesting that yellow patches were a response to PS–NH_2 >25 μg mL^{-1}. While the identity of these patches remains to be investigated, we posit that they result from siderophore production as previously shown in *P. defensor*. Siderophores primarily scavenge iron under iron-limiting conditions and enhanced resistance to oxidative stress in other Gram-negative bacteria. Given that biofilms were grown in nutrient-rich media (Fig. 4A), siderophore production

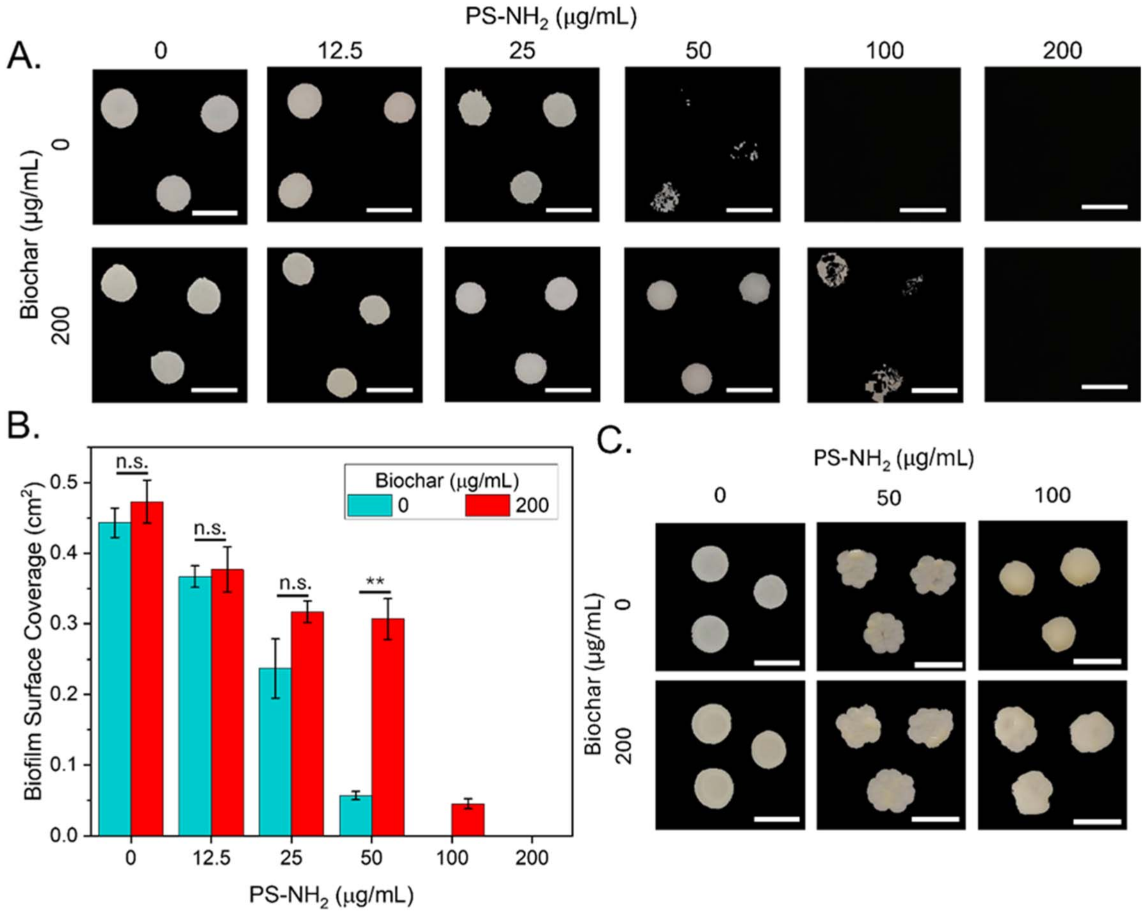

Fig. 4 Biofilms on agar and surface coverage after nanoplastic conditioning with biochar. (A) 1 d biofilms on agar after exposure to PS–NH_2 without or with prior exposure of 200 μg per mL biochar. Scale: 1 cm. (B) Average biofilm surface coverage after 1 d growth on agar. Bars represent standard deviation of at least three biofilms and experiments were repeated at least three times, where ** represents $p < 0.01$ from t-test. (C) 3 d biofilms on agar after exposure to 0, 50 and 100 μg per mL PS–NH_2 with or without biochar. Biofilm images were taken from the top of the agar plate.

in *P. defensor* biofilms was likely a response to oxidative stress, not iron-limitation. We argue that this is plausible since PS–NH_2 is known to induce oxidative stress in bacteria.[26] Since biochar significantly sequestered PS–NH_2 (Fig. 1 and 2), this could explain why biofilms were less yellow than biofilms without biochar and suggests biochar might reduce oxidative stress in biofilm (Fig. 4C).

Overall, biochar facilitates the early recovery of planktonic growth at lower nanoplastic concentrations, while its role in enhancing biofilm resilience is only significant during early biofilm formation at higher nanoplastic levels. In contrast, simultaneous exposure of bacteria to biochar and nanoplastic could not significantly improve planktonic growth, biofilms at 50 μg mL^{-1} were deformed and biofilms were completely inhibited at 100 μg mL^{-1} (Fig. S13). Similarly, negatively charged nanoplastic did not affect bacterial growth (Fig. S14). However, further research is necessary into how transport and transformation of nanoplastic in soil environments can impact microbes in the rhizosphere. For example, nanoparticle mobility may be influenced by water content, rainwater, and bioturbation which might lead to microbe interactions.[43,44] Similarly, oxidation can lead to aging-induced changes to particle morphology and chemistry. Therefore, our results using negatively charged plastic are relevant where freshly deposited particles have not yet undergone extensive oxidative aging. However, the premise of some reports is that functionalization already represents aging relative to pristine nanoparticles.[45] Currently, our lab is investigating growth mechanisms in different environments as prior observations suggested active removal of PS–NH_2 before growth could resume.[20]

Conclusion

Our work demonstrates that pre-conditioning polystyrene nanoplastic with biochar can significantly mitigate their toxicity towards plant growth-promoting bacteria and improve maximum growth, lag phase, and biofilm formation. However, when bacteria simultaneously encounter PS–NH_2 and biochar, biochar no longer improves bacterial growth or biofilm formation. While biochar can also immobilize bare PS, PS–SO_4 and PS–COO^-, negatively charged nanoplastic have no negative impact towards bacterial growth or biofilm formation due to lack of membrane binding.

Biochar is widely recognized as a valuable agricultural amendment due to its positive effects on soil and soil biota. However, there is a critical lack of understanding regarding how biochar interacts with emerging nanomaterial pollutants and their combined impact on bacteria. Although biochar can enhance soil health and support bacterial communities, the role of nanoplastics in influencing these interactions is not yet well understood. Our study highlights conditions where biochar may be effective and ineffective for bacterial growth and biofilm formation under environments with emerging nanomaterials such as nanoplastic. A one-step application of biochar may not be effective for improving the growth of rhizobacteria since nanoplastic might outcompete biochar for binding bacteria. Our study suggests a two-step approach, where the application of biochar to plastic-contaminated soil would first serve to sequester nanoplastic, followed by the second step, where the application of bacterial biofertilizer could lead to better growth compared to the one-step approach.

Author contributions

F. P. conceived, designed, performed experiments and analyzed the data. Y. C. and C. J. prepared and characterized the biochar and helped conceive the study. D. Y. and J. H. carried out SEM imaging and assisted in the analysis of biochar–nanoplastic interactions. T. S. S. analyzed some data and prepared the figures. R. M. A. S. initiated the project and edited the final version of the manuscript. All authors have given approval to the final version of the manuscript.

Conflicts of interest

There are no conflicts to declare.

Data availability

The data supporting this article have been included as part of the SI, which includes the following: (i) characterization of nanoplastic, bacteria, and biochar. (ii) Fluorescence intensity controls for nanoplastics. (iii) Interaction of negatively charged nanoplastics with biochar. (iv) Characterization of nanoplastics after interaction with biochar. (v) Additional confocal images of bacteria after interaction with nanoplastics and biochar. (vi) Confocal images of bacteria after interaction with negatively charged nanoplastics. (vii) Bacterial growth rate and lag phase after exposure to nanoplastics and biochar. (viii) Planktonic growth parameters and biofilm formation on agar after simultaneous exposure to nanoplastics and biochar. (ix) Growth curves and biofilm images after exposure to negatively charged nanoplastics. (x) FTIR on bacteria, nanoplastic, and biochar. (xi) Bacterial growth under additional media. (xii) Fluorescence intensity, hydrodynamic diameter, and surface charge as a function of temperature and salinity. (xiii) Fluorescence intensity data at higher biochar concentrations. See DOI: **https://doi.org/10.1039/d5ra02482j**.

Acknowledgements

This research was funded by the Natural Science and Engineering Research Council Canada (NSERC, RGPIN-2017-06522) and Research Corporation for Science Advancement (Cottrell Faculty Scholar Award). We acknowledge Durga Acharya and Bruno Chue from the Centre for the Neurobiology of Stress at the University of Toronto Scarborough for assistance in confocal microscopy and SEM imaging.

References

1 E. D. Okoffo, S. O'Brien, F. Ribeiro, S. D. Burrows, T. Toapanta, C. Rauert, J. W. O'Brien, B. J. Tscharke, X. Y. Wang and K. V. Thomas, *Environ. Sci.:Processes Impacts*, 2021, **23**, 240–274.
2 J. Gigault, H. El Hadri, B. Nguyen, B. Grassl, L. Rowenczyk, N. Tufenkji, S. Feng and M. Wiesner, *Nat. Nanotechnol.*, 2021, **16**, 501–507.
3 K. K. Verma, X. P. Song, L. Xu, H. R. Huang, Q. Liang, C. S. Seth and Y. R. Li, *Front. Plant Sci.*, 2023, **14**, 1283852.
4 P. R. Rout, A. Mohanty, Aastha, A. Sharma, M. Miglani, D. Z. Liu and S. Varjani, *J. Hazard. Mater. Adv.*, 2022, **6**, 100070.
5 F. A. Olabemiwo, A. Hagan, M. Cham and F. M. Cohan, *Sci. Total Environ.*, 2024, **907**, 167972.
6 S. A. Howard and R. R. McCarthy, *npj Biofilms Microbiomes*, 2023, **9**, 72.
7 S. Yoshida, K. Hiraga, T. Takehana, I. Taniguchi, H. Yamaji, Y. Maeda, K. Toyohara, K. Miyamoto, Y. Kimura and K. Oda, *Science*, 2016, **351**, 1196–1199.
8 T. Nomura, E. Fujisawa, S. Itoh and Y. Konishi, *J. Nanopart. Res.*, 2016, **18**, 157.
9 Z. F. Yu, X. L. Xu, L. Guo, R. Jin and Y. Lu, *Sci. Total Environ.*, 2024, **907**, 168155.
10 W. K. Yuan, E. G. Xu, S. Shabaka, P. Chen and Y. Y. Yang, *Eco-Environ. Health*, 2024, **3**, 260–265.
11 Y. W. Zhou, M. Kumar, S. Sarsaiya, R. Sirohi, S. K. Awasthi, R. Sindhu, P. Binod, A. Pandey, N. S. Bolan, Z. Q. Zhang, L. Singh, S. Kumar and M. K. Awasthi, *Sci. Total Environ.*, 2022, **802**, 149823.
12 G. Y. Ji, Y. C. Xing and T. Y. You, *J. Environ. Chem. Eng.*, 2024, **12**, 113377.
13 R. Kumar, A. Verma, M. R. J. Rakib, P. K. Gupta, P. Sharma, A. Garg, P. Girard and T. M. Aminabhavi, *Sci. Total Environ.*, 2023, **856**, 159097.
14 Y. Shi, J. D. Du, T. M. Zhao, B. Feng, H. H. Bian, S. D. Shan, J. Meng, P. Christie, M. H. Wong and J. Zhang, *Environ. Pollut.*, 2023, **318**, 120897.
15 Z. A. Ganie, N. Khandelwal, E. Tiwari, N. Singh and G. K. Darbha, *J. Hazard. Mater.*, 2021, **417**, 126096.
16 Y. Yu and J. Li, *Sci. Total Environ.*, 2024, **906**, 167258.
17 R. A. Hill, J. Hunt, E. Sanders, M. Tran, G. A. Burk, T. E. Mlsna and N. C. Fitzkee, *Environ. Sci. Technol.*, 2019, **53**, 2635–2646.

18 H. Yan, M. F. Cong, Y. Hu, C. C. Qiu, Z. L. Yang, G. M. Tang, W. L. Xu, X. P. Zhu, X. Sun and H. T. Jia, *Front. Microbiol.*, 2022, **13**, 1023444.
19 N. Singh, N. Khandelwal, Z. A. Ganie, E. Tiwari and G. K. Darbha, *Chem. Eng. J.*, 2021, **418**, 129405.
20 F. Perez, N. M. O. Andoy, U. T. T. Hua, K. Yoshioka and R. M. A. Sullan, *Environ. Sci.:Nano*, 2025, **12**, 1477–1486.
21 R. S. Gabhi, D. W. Kirk and C. Q. Jia, *Carbon*, 2017, **116**, 435–442.
22 R. Gabhi, K. Tan, T. J. Feng, D. W. Kirk, M. Giorcelli, A. Tagliaferro and C. Q. Jia, *Biomass Bioenergy*, 2024, **181**, 107051.
23 N. M. O. Andoy, K. Jeon, C. T. Kreis and R. M. A. Sullan, *Adv. Funct. Mater.*, 2020, **30**, 2004503.
24 J. Schindelin, I. Arganda-Carreras, E. Frise, V. Kaynig, M. Longair, T. Pietzsch, S. Preibisch, C. Rueden, S. Saalfeld, B. Schmid, J. Y. Tinevez, D. J. White, V. Hartenstein, K. Eliceiri, P. Tomancak and A. Cardona, *Nat. Methods*, 2012, **9**, 676–682.
25 M. H. Shihan, S. G. Novo, S. J. Le Marchand, Y. Wang and M. K. Duncan, *Biochem. Biophys. Rep.*, 2021, **25**, 100916.
26 R. Y. Wang, X. D. Li, J. Li, W. Dai and Y. N. Luan, *Fermentation*, 2023, **9**, 939.
27 H. S. Kambo and A. Dutta, *Renewable Sustainable Energy Rev.*, 2015, **45**, 359–378.
28 A. Pradel, C. Catrouillet and J. Gigault, *NanoImpact*, 2023, **29**, 100453.
29 T. Nomura, Y. Kuriyama, H. Tokumoto and Y. Konishi, *J. Nanopart. Res.*, 2015, **17**, 105.
30 Z. V. Feng, I. L. Gunsolus, T. A. Qiu, K. R. Hurley, L. H. Nyberg, H. Frew, K. P. Johnson, A. M. Vartanian, L. M. Jacob, S. E. Lohse, M. D. Torelli, R. J. Hamers, C. J. Murphy and C. L. Haynes, *Chem. Sci.*, 2015, **6**, 5186–5196.
31 D. Sharan, D. Wolfson, C. M. Green, P. Lemke, A. G. Gavin, R. J. Hamers, Z. V. Feng and E. E. Carlson, *Environ. Sci.:Nano*, 2023, **10**, 1978–1992.
32 K. H. Jacobson, I. L. Gunsolus, T. R. Kuech, J. M. Troiano, E. S. Melby, S. E. Lohse, D. Hu, W. B. Chrisler, C. J. Murphy, G. Orr, F. M. Geiger, C. L. Haynes and J. A. Pedersen, *Environ. Sci. Technol.*, 2015, **49**, 10642–10650.
33 S. K. Manikandan and V. Nair, *New J. Chem.*, 2023, **47**, 21199–21213.
34 B. F. Zhang, L. Zhang and X. X. Zhang, *RSC Adv.*, 2019, **9**, 35304–35311.
35 K. Sonsuphab, W. Toomsan, N. Supanchaiyamat, A. J. Hunt, Y. Ngernyen, T. Ratpukdi and S. Siripattanakul-Ratpukdi, *J. Environ. Chem. Eng.*, 2022, **10**, 107610.
36 Q. Y. Shi, S. S. Guo, J. C. Tang, H. Lyu, C. Ri and H. W. Sun, *Environ. Pollut.*, 2023, **316**, 120696.
37 F. Y. Fu, S. Wang, X. R. Zhang, Y. Xia, H. Deng, Y. Y. Zhao, Y. Zhang and C. J. Ge, *J. Environ. Chem. Eng.*, 2025, **13**, 115551.
38 R. Saila and B. R. Dhar, *Sci. Total Environ.*, 2024, **957**, 177589.
39 M. Sun, X. Z. Wang, R. Y. Xiong, X. Y. Chen, L. F. Zhai and S. B. Wang, *Sci. Total Environ.*, 2023, **901**, 165971.
40 N. Zhu, Q. Yan, Y. P. He, X. Y. Wang, Z. A. Wei, D. Liang, H. F. Yue, Y. Yun, G. K. Li and N. Sang, *J. Hazard. Mater.*, 2022, **433**, 128756.
41 A. Bhattacharyya, O. Mavrodi, N. Bhowmik, D. Weller, L. Thomashow and D. Mavrodi, *Biofilms*, 2023, **53**, 3–48.
42 N. Ajijah, A. Fiodor, A. K. Pandey, A. Rana and K. Pranaw, *Diversity*, 2023, **15**, 112.
43 R. Perez-Reveron, S. J. Alvarez-Mendez, J. Gonzalez-Salamo, C. Socas-Hernandez, F. J. Diaz-Pena, C. Hernandez-Sanchez and J. Hernandez-Borges, *Environ. Pollut.*, 2023, **317**, 120788.
44 W. M. Heinze, D. M. Mitrano, E. Lahive, J. Koestel and G. Cornelis, *Environ. Sci. Technol.*, 2021, **55**, 16423–16433.
45 F. Pirade, J. W. Foppen, J. P. van der Hoek and K. M. Lompe, *Environ. Pollut.*, 2025, **366**, 125393.